LAWRENCE
LIVERMORE
NATIONAL
LABORATORY

UCRL-JRNL-208737

# The Impact of humidity above stratiform clouds on indirect aerosol climate forcing

A. S. Ackerman, M. P. Kirkpatrick, D. E. Stevens, O. B. Toon

December 21, 2004

Nature

# The impact of humidity above stratiform clouds on indirect aerosol climate forcing

Andrew S. Ackerman[1], Michael P. Kirkpatrick[2], David E. Stevens[3], Owen B. Toon[4]

[1]NASA Ames Research Center, Moffett Field, CA 94035, USA
[2]University of Tasmania, Hobart, TAS 7001, Australia
[3]Lawrence Livermore National Laboratory, Livermore, CA 94552, USA
[4]University of Colorado, Boulder, CO 80309, USA

**Some of the global warming effect of anthropogenic greenhouse gases is offset by increased solar reflection from clouds with smaller droplets that form on increased numbers of cloud condensation nuclei in polluted air[1]. The global magnitude of the resulting indirect aerosol climate forcing is estimated to be comparable (and opposed) to the anthropogenic carbon dioxide forcing, but estimates are highly uncertain because of complexities in characterizing the physical process that determine global aerosol and cloud populations and their interactions[2]. Beyond reflecting sunlight more effectively, smaller droplets are less efficient at producing precipitation, and decreased precipitation is expected to result in increased cloud water and cloud cover[3, 4], further increasing the indirect forcing. Yet polluted marine boundary-layer clouds are not generally observed to hold more water[5, 6, 7]. Here we use model simulations of stratocumulus clouds to show that suppression of precipitation from increased droplet concentrations leads to increased cloud water only when sufficient precipitation reaches the surface, a condition favored when the overlying air is moist. Otherwise, aerosol induced suppression of precipitation enhances entrainment of overlying dry air, thereby reducing cloud water and diminishing the indirect climate forcing.**

Measuring the response of cloud water to changes in aerosol and droplet concentrations is extremely challenging because aerosol abundance typically covaries with meteorological conditions, making it difficult to separate the microphysical and meteorological signals. For instance, when a regional-scale pollution plume flows offshore, cloud properties will respond to not only the aerosol abundance but also the dryness of the plume[8].

Ship tracks, which are plumes of enhanced albedo in clouds polluted by ship exhaust, provide a natural laboratory for isolating the effects of aerosol changes on cloud properties. Results from simple theoretical models[3, 4] suggest that cloud water should consistently increase in ship tracks, an expectation not generally confirmed by observations. The first reported airborne measurements of ship tracks[9] support the theoretical expectations, with cloud water nearly doubling as droplet concentrations ($N$) tripled from their background values of $\sim$30 cm$^{-3}$. Subsequent observations, however, tend to show just the opposite relationship, if any, with cloud water generally *decreasing* as droplet concentrations increase. For example, in situ measurements of over 60 ship-track interceptions during the MAST field project off the coast of central California show that cloud water increases in some and decreases in others, with a slight decrease on average[5]. High-resolution, airborne remote-sensing of three ship tracks during MAST also showed cloud water decreasing on average[6]. More recently, satellite observations of hundreds of ship tracks over the northeastern Pacific Ocean show a significant average decrease in cloud water[7].

Here we investigate the dependence of cloud water on droplet concentrations using model simulations based on stratocumulus measurements during three field projects: (1) a nocturnal case study of drizzling clouds over the northeastern Atlantic during ASTEX[10, 11]; (2) a nocturnal study during DYCOMS-II off the coast of southern California[12], with very light precipitation largely limited to the cloud deck[13]; and (3) an idealization of cloudy conditions measured over two days during FIRE-I, also off the coast of southern California. For each meteorological setting we ran a sequence of 8-h nocturnal model simulations (daytime simulations are discussed subsequently) in which only the aerosol concentration was varied. As seen in Figure 1, only when the average precipitation rate at the surface exceeds $\sim$0.1 mm d$^{-1}$ does the average liquid water path

(LWP) increase with droplet concentrations in the simulations. This drizzling regime is consistent with simple models[3, 4] in which decreased drizzle allows LWP to increase. An increase of LWP with droplet concentrations is seen for the ASTEX simulations over the entire range of aerosol concentrations considered (40–600 $cm^{-3}$, corresponding to average droplet concentrations of 25–350 $cm^{-3}$). For the DYCOMS-II and FIRE-I conditions LWP again increases with $N$, but only below droplet concentrations of $\sim$35 and 225 $cm^{-3}$, respectively.

These increases in LWP with $N$ occur despite an increase with $N$ in the rate at which the boundary layer entrains dryer air from above. The entrainment rate always increases with $N$ in our simulations (Figure 1), consistent with theoretical arguments[14]: divergence of the precipitation flux dries out cloudy air near cloud-top, which reduces the moisture available to evaporatively cool downdrafts. Precipitation thus decreases the kinetic energy available in the boundary layer to entrain warmer air from above the temperature inversion. Conversely, a reduction in precipitation accelerates entrainment.

The response of LWP to increasing droplet concentrations can be considered as a competition between the effects of precipitation at the surface and near cloud-top. Decreased precipitation at the surface tends to increase LWP, while decreased precipitation near cloud-top tends to increase entrainment and thus decrease LWP. Only when the surface precipitation is sufficiently strong can it dominate the LWP response.

Precipitation depends on a number of environmental factors, and the three cases we consider here differ in a number of ways (see Table 1 and Methods). We find that the humidity of air overlying the boundary layer exerts a strong control on the surface precipitation rate. Moist air above the boundary layer is conducive to drizzle and thus favors the effect of precipitation at the surface: in the case of ASTEX the relative humidity above the boundary layer is $\sim$70% and LWP monotonically increases with $N$ over the range of aerosol and droplet concentrations we consider (Figure 1). In contrast, entrainment of dry air above the boundary layer reduces cloud water and thereby suppresses drizzle, lowering the droplet concentration above which the entrainment effect of precipitation dominates changes in cloud water with $N$. In the case of DYCOMS-II, with

a relative humidity of $\sim$10%, LWP decreases as $N$ increases, except at extremely low droplet concentrations. In the intermediate case of FIRE-I, with a relative humidity close to 40%, LWP is seen to increase with $N$ only at low-to-moderate droplet concentrations, and reverses at higher droplet concentrations.

To isolate the role of humidity above the boundary layer, we ran another sequence of simulations using the ASTEX meteorology, modified with warmer, dryer air above the boundary layer. In addition to decreasing the water vapor we also increased the temperature above the boundary layer to avoid stratocumulus breakup from cloud-top entrainment instability (see Supplemental Figure 1). The relative humidity above the boundary layer is $\sim$25% in the modified conditions, substantially reducing precipitation and resulting in LWP decreasing as droplet concentrations increase beyond 70 cm$^{-3}$ (Figure 1). Thus we find that modifying the relative humidity above the boundary layer profoundly alters the balance between the competing effects of precipitation on LWP.

To further clarify the physics underlying the different responses of LWP to increasing droplet concentrations, we also ran simulations in which sedimentation of water is prevented. As seen in Figure 2, drizzle reaches the surface for the ASTEX simulations (as observed), providing leverage for the effect of surface precipitation on LWP. Inhibiting precipitation results in the boundary layer moistening and LWP increasing as found in simpler models[3, 4]. Suppressing drizzle does increase entrainment, but the entrained air is moist and ineffective at drying the boundary layer, and the cloud layer deepens as cloud base sharpens.

For the ASTEX simulations with the same aerosol concentration but with the relative humidity reduced above the boundary layer, precipitation is drastically reduced by the entrainment of dry air. Because precipitation does not reach the surface for these conditions, it cannot be reduced further, and thus surface precipitation has no leverage on LWP. There is droplet sedimentation within the cloud layer, however, and a sedimentation flux divergence at cloud top. Completely suppressing this sedimentation accelerates entrainment, drying the boundary layer and thinning the cloud layer as cloud base rises faster than cloud top. We have also run simulations of daytime conditions,

which show smaller trends in LWP as droplet concentrations increase. By offsetting longwave radiative cooling that drives stratocumulus convection, solar heating reduces convective mixing and results in a decreased response of LWP to microphysical changes (see Supplemental Table 1). Reduction of the wind strength reduces the generation of turbulent mixing by shear, and also results in a decreased response (Supplemental Table 1). We also find that our results have effectively converged (with respect to grid spacing) on the grid mesh we use here (see Supplemental Figure 2).

There are a number of implications of our findings. Regarding the response of cloud water to changes in droplet concentrations, our analysis suggests that the very concept of "non-precipitating clouds" can be misleading. For cases in which little or no precipitation falls from a cloud layer, it is a mistake to assume that sedimentation of droplets within the cloud layer has no effect on entrainment and thus cloud water. To the contrary, it is the change in the precipitation flux from droplet sedimentation within such clouds that modulates the drying of the boundary layer by entrainment.

Our results also show how cloud water can be depressed in clouds polluted by aerosol particles acting as cloud nuclei, and the mechanism we describe here may well explain the decrease in LWP observed in high-resolution imagery of ship tracks[6]. (Although we find no reason to contest the argument that omitting partly-cloudy and clear pixels introduces a sampling bias that can lead to misleading conclusions[15].) Because of the difficulties in accurately retrieving surface precipitation rates below stratocumulus using satellite measurements, we recommend that satellite retrievals of cloud microphysics (not limited to overcast pixels) be combined with meteorological analyses to assess the hypothesis we put forth here regarding the dependence of LWP tendencies on humidity above the boundary layer.

In contrast to one-dimensional models that include drizzle but not the effect of cloud droplet sedimentation on entrainment[3, 4], our simulations show that LWP can decrease as droplet concentrations increase. Other models that treat cloud droplet sedimentation show that when convective mixing is suppressed by strong solar heating, LWP can decrease as $N$ increases in stratocumulus with very light precipitation[16, 17]. Those studies, however, were each limited to single meteorological settings, and did not address the role of humidity above the boundary layer. By considering

a variety of meteorological settings, here we identify relative humidity above the boundary layer as a leading factor determining the response of cloud water to changes in droplet concentrations. When the air above the boundary layer is dry, we find that LWP decreases as $N$ increases even in nocturnal simulations (and equivalently, in the morning or seasons or latitudes where sunlight is weak). Beyond marine stratocumulus, we recommend investigating the effect of overlying humidity on the response of cloud water to changes in droplet concentrations in other cloud types, such as continental and mixed-phase stratiform clouds, as well as in transitions between cloud regimes.

In light of our findings, global estimates from satellite observations of the indirect aerosol forcing in boundary-layer clouds[18] require estimating not only the regional changes in cloud droplet concentrations, but also the co-varying climatologies in relative humidity above stratocumulus regions. Also, predictions of climate change require global climate models to accurately represent such critical details as boundary-layer entrainment, a notoriously challenging problem, as well as its response to changes in cloud droplet sedimentation. We speculate that our results may help to explain why forward climate models, which consistently show an amplification of the "Twomey effect"[19], tend to overestimate the overall indirect aerosol forcing compared to inverse calculations from simpler models constrained by the historical temperature record[20].

**Methods**

**Model description**

The fluid dynamics model is described by Stevens and co-authors[21]. The computational domain extends 3.2 km in both horizontal directions and 1.5 km vertically (1 km for the FIRE-I simulations), with $64 \times 64 \times 86$ cells in the $x, y$ and $z$ directions respectively. Grid spacing is uniform horizontally and stretched vertically to give cells of height 6 m close to the surface and in the vicinity of the inversion. The model domain is translated with the geostrophic winds, thereby reducing numerical errors associated with advection. A sponge layer occupies the upper 250 m of the domain. Sub-grid scale fluxes are modeled using a dynamic turbulence model[22]. A modified version of the Brown et al.[23] model is used to treat surface-layer stresses in the bottom 100 m of the domain. Effects of latent heat exchange on sub-grid scale buoyancy follow MacVean and Mason[24].

Subsidence and radiative forcings are linearly attenuated to zero in the 300 m above the inversion (defined as the average height where the total water mixing ratio exceeds a threshold that depends on the meteorological scenario) to prevent drift of the overlying atmospheric properties resulting from any unbalanced forcings[25]. The cloud microphysics model is described by Ackerman and co-authors[26] and the linkages with the fluid dynamics model are described by McFarlane and co-authors[27]. Particle size distributions are resolved into 20 bins over a range from 0.01 to 4.3 $\mu$m radius for dry condensation nuclei, which are assumed to consist of ammonium bisulfate, and over a range from 1 to 430 $\mu$m radius for activated cloud droplets. The total particle number concentration at each grid point is fixed in each simulation[27]. The aerosol distributions are log-normal with a geometric mean radius of 0.1 $\mu$m and a geometric standard deviation of 1.5. Radiative transfer is calculated for each column once every minute with a two-stream model[28].

**Setup of model simulations**

The ASTEX simulations are based on an idealization of the 12-13 June 1992 nocturnal stratocumulus measurements obtained by the U.K. Meteorological Research Flight C-130 aircraft (flight A209) of the Atlantic Stratocumulus Transition Experiment[10, 11], with model initialization and forcings adapted from the 4th Global Energy and Water Experiment (GEWEX) Cloud System Studies (GCSS) Boundary Layer Cloud Workshop (12-16 August 1996, Clermont-Ferrand, France). We depart from the workshop specifications by initializing our model domain as initially cloud free and using surface similarity for surface fluxes, with the sea surface temperature fixed at 292.4 K. As done in the 8th GCSS Boundary Layer Cloud Workshop (see below), the fluxes of heat and moisture are fixed during the first two hours, in this case at 10 and 30 W m$^{-2}$, respectively. In place of the radiative flux parameterization in the workshop specification we use a two-stream radiative transfer model in which the precipitable water vapor overlying the model domain is fixed at 2.2 cm, resulting in a net (upward) longwave flux of 70 W m$^{-2}$ above the boundary layer after the cloud layer forms. For the "dry ASTEX" simulations the surface moisture flux during the first two hours is increased to 60 W m$^{-2}$ and the overlying precipitable water vapor is increased to 3.2 cm. The inversion height is defined as the average altitude where the total water mixing ratio is 8 g

$kg^{-1}$.

The DYCOMS-II simulations are based on an idealization of nocturnal stratocumulus observations obtained during the first research flight of the second Dynamics and Chemistry of Marine Stratocumulus field study[13], with model initialization and forcings adapted from the step 4 of the 8th GCSS Boundary Layer Cloud Workshop (29-31 October, 2003, Broomfield, Colorado, USA). The precipitable water vapor overlying the model domain is fixed at 1.85 cm, resulting in a net longwave flux of 80 W $m^{-2}$ above the boundary layer after the cloud layer forms. The total water mixing ratio defining the inversion height is 8 g $kg^{-1}$.

The FIRE-I simulations are based on an idealization of stratocumulus observations obtained during 14 and 15 July 1987 of the First ISCCP (International Satellite Cloud Climatology Project) Regional Experiment with model initialization and forcings adapted from the EUROCS (European Project on Cloud Systems in Climate Models) stratocumulus case (submitted manuscript by P. G. Duynkerke, S. R. deRoode, et al.). Here we use a large-scale divergence rate of $5 \times 10^{-6}$ $s^{-1}$ and ignore any large-scale advective forcings. The fluxes of heat and moisture during the first two hours are fixed at 5 and 24 W $m^{-2}$, respectively. The precipitable water vapor overlying the model domain is fixed at 2 cm, resulting in a net longwave flux of 75 W $m^{-2}$ above the boundary layer after the cloud layer forms. The total water mixing ratio defining the inversion height is 9 g $kg^{-1}$.

# References


1. Twomey, S. Pollution and the planetary albedo. *Atmos. Environ.* **8**, 1251–1256 (1974).

2. Houghton, J. T. et al., editors. *Climatic Change 2001: The Scientific Basis*. Cambridge University Press, (2001).

3. Albrecht, B. Aerosols, cloud microphysics, and fractional cloudiness. *Science* **245**, 1227–1230 (1989).

4. Pincus, R. and Baker, M. B. Effect of precipitation on the albedo susceptibility of clouds in the marine boundary layer. *Nature* **312**, 250–242 (1994).

5. Ackerman, A. S. et al. Effects of aerosols on cloud albedo: Evaluation of Twomey's parameterization of cloud susceptibility using measurements of ship tracks. *J. Atmos. Sci.* **57**, 2684–2695 (2000).

6. Platnick, S. et al. The role of background cloud microphysics in the radiative formation of ship tracks. *J. Atmos. Sci.* **57**, 2607–2624 (2000).

7. Coakley, Jr., J. A. and Walsh, C. D. Limits to the aerosol indirect radiative effect derived from observations of ship tracks. *J. Atmos. Sci.* **59**, 668–680 (2002).

8. Brenguier, J. L., Pawlowska, H., Schüller, L., Preusker, R., Fischer, J., and Fouquart, Y. Radiative properties of boundary layer clouds: Droplet effective radius versus number concentration. *J. Atmos. Sci.* **57**, 803–821 (2000).

9. Radke, L. F., J. A. Coakley, J., and King, M. D. Direct and remote sensing observations of the effects of ships on clouds. *Science* **246**, 1146–1149 (1989).

10. Duynkerke, P. G., Zhang, H., and Jonker, P. J. Microphysical and turbulent structure of nocturnal stratocumulus as observed during ASTEX. *J. Atmos. Sci.* **52**, 2763–2777 (1995).

11. Bretherton, C. S., Austin, P., and Siems, S. T. Cloudiness and marine boundary layer dynamics in the ASTEX Lagrangian experiments: Part II: Cloudiness, drizzle, surface fluxes, and entrainment. *J. Atmos. Sci.* **52**, 2724–2735 (1995).

12. Stevens, B. et al. On entrainment rates in nocturnal marine stratocumulus. *Quart. J. Roy. Meteor. Soc.* **595**, 3469–3494 (2003).

13. Stevens, B. et al. Dynamics and chemistry of marine stratocumulus – DYCOMS-II. *Bull. Amer. Meteor. Soc.* **84**, 579–593 (2003).

14. Stevens, B., Cotton, W. R., Feingold, G., and Moeng, C.-H. Large-eddy simulations of strongly precipitating, shallow, stratocumulus-topped boundary layers. *J. Atmos. Sci.* **55**, 3616–3638 (1998).

15. Ackerman, A. S., Toon, O. B., Stevens, D. E., and J. A. Coakley, J. Enhancement of cloud cover and suppression of noctural drizzle in stratocumulus polluted by haze. *Geophys. Res. Lett.* **30(7)**, 1381 (2003).

16. Ackerman, A. S., Toon, O. B., and Hobbs, P. V. Numerical modeling of ship tracks produced by injections of cloud condensation nuclei into marine stratiform clouds. *J. Geophys. Res.* **100(D4)**, 7121–7133 (1995).

17. Jiang, H., Feingold, G., and Cotton, W. R. Simulations of aerosol-cloud-dynamical feedbacks resulting from entrainment of aerosol into the marine boundary layer during the Atlantic Stratocumulus Transition Experiment. *J. Geophys. Res.* **107(D24)**, 4813 (2002).

18. Nakajima, T., Higurashi, A., Kawamoto, K., and Penner, J. E. A possible correlation between satellite-derived cloud and aerosolmicophrophysical parameters. *Geophys. Res. Lett.* **28**, 1171–1174 (2001).

19. Haywood, J. and Boucher, O. Estimates of the direct and indirect radiative forcing due to tropospheric aerosols: A review. *Rev. Geophys.* **38**, 513–543 (2000).

20. Knutti, R., Stocker, T. F., Joos, F., and Plattner, G.-K. Constraints on radiative forcing and future climate change from observations and climate model ensembles. *Nature* **416**, 719–723 (2002).

21. Stevens, D. E., Ackerman, A. S., and Bretherton, C. S. Effect of domain size and numerical resolution on the simulation of shallow cumulus convection. *J. Atmos. Sci.* **59**, 3285–3301 (2002).

22. Germano, M., Piomelli, U., Moin, P., and Cabot, W. H. A dynamic subgrid-scale viscosity model. *Phys. Fluids A* **3**, 1760–1765 (1991).

23. Brown, A. R., Hobson, J. M., and Wood, N. Large-eddy simulation of neutral turbulent flow over rough sinusoidal ridges. *Bound.-Layer Meteor.* **98**, 411–441 (2001).

24. MacVean, M. K. and Mason, P. J. Cloud-top entrainment instability through small-scale mixing and its parameterization in numerical models. *J. Atmos. Sci.* **47**, 1012–1030 (1990).

25. Stevens, B. et al. Trade-wind cumuli under a strong inversion. *J. Atmos. Sci.* **58**, 1870–1891 (2001).

26. Ackerman, A. S., Toon, O. B., and Hobbs, P. V. A model for particle microphysics, turbulent mixing, and radiative transfer in the stratocumulus-topped marine boundary layer and comparisons with measurements. *J. Atmos. Sci.* **52**, 1204–1236 (1995).

27. McFarlane, S., Evans, F., and Ackerman, A. S. A Bayesian algorithm for the retrieval of liquid water cloud properties from microwave radiometer and millimeter radar data. *J. Geophys. Res.* **107(D16)**, 4317 (2002).

28. Toon, O. B., McKay, C. P., Ackerman, T. P., and Santhaman, K. Rapid calculation of radiative heating and photodissociation rates in inhomogeneous multiple scattering atmospheres. *J. Geophys. Res.* **94**, 16287–16301 (1989).

**Acknowledgements** We thank Ann Fridlind and Eric Jensen for helpful comments on the manuscript, Nagi Mansour, Joel Ferziger, and Robert Street for helpful discussions regarding the sub-grid scale model, and Bjorn Stevens for providing the DYCOMS-II measurements to the 8th GCSS Boundary Layer Cloud Workshop. This work was supported by the Radiation Science Program of NASA.

**Competing interests statement** The authors declare that they have no competing financial interests.

**Correspondence** and requests for material should be addressed to A.S.A. (andrew.ackerman@nasa.gov).

This work was performed under the auspices of the U.S. Department of Energy by University of California, Lawrence Livermore National Laboratory under contract W-7405-Eng-48.

Table 1 **Meteorological conditions used for stratocumulus simulations**

| | ASTEX | FIRE-I | DYCOMS-II |
|---|---|---|---|
| Sea surface temperature (K) | 290.4 | 289.0 | 292.5 |
| Lifting condensation level (m) | 340 | 250 | 620 |
| Geostrophic wind speed (m $s^{-1}$) | 10 | 6 | 9 |
| Inversion height (m) | 700 | 600 | 840 |
| Temperature increase across inversion (K)* | 5.5 | 12 | 10 |
| Moisture decrease across inversion (g $kg^{-1}$) | 1.0 | 3.0 | 7.5 |
| Relative humidity above inversion (%) | 70 | 40 | 25 |

*Difference in liquid water potential temperature above and below the temperature inversion capping the boundary layer.

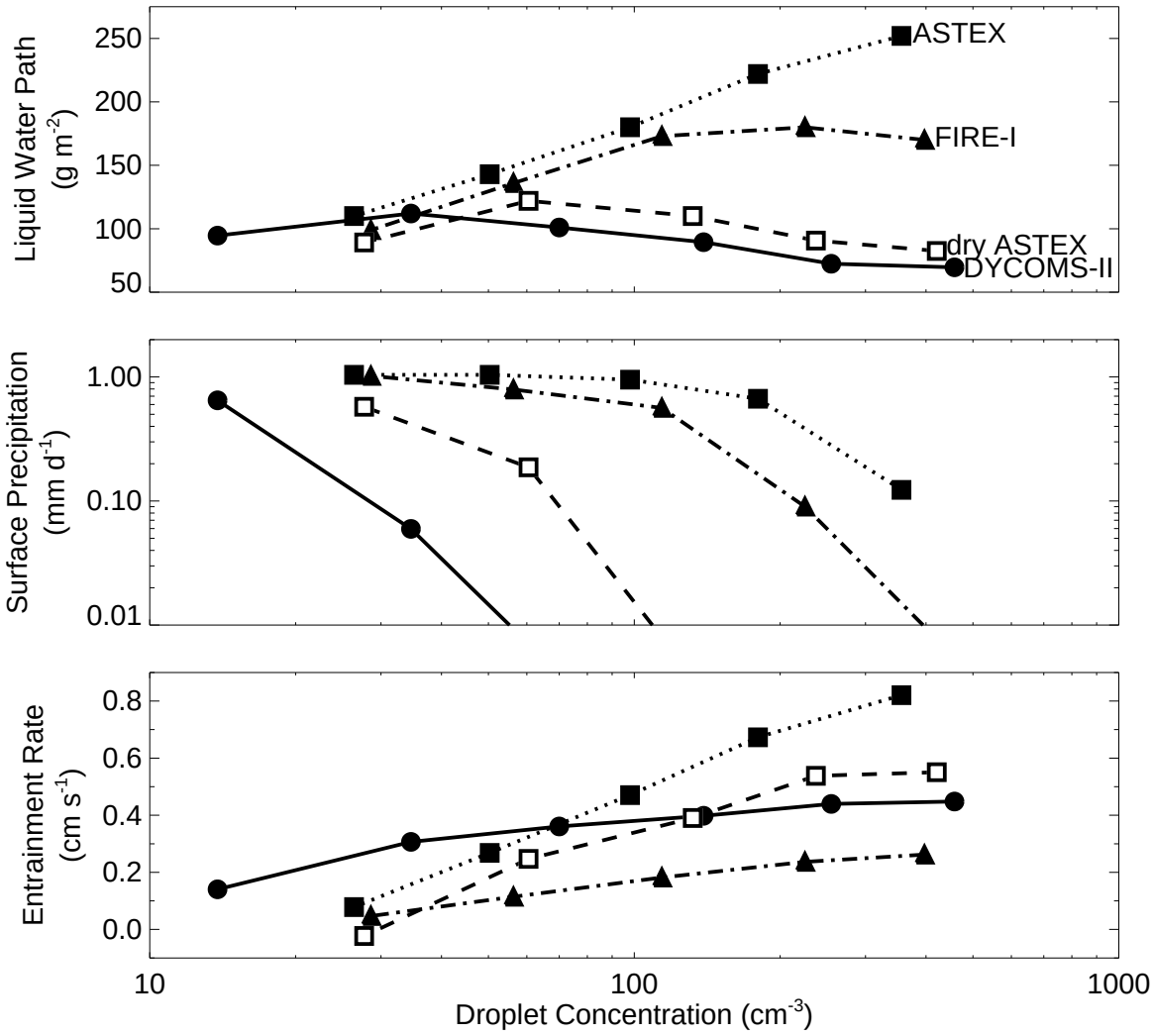


Figure 1: Domain average liquid water path, surface precipitation, and entrainment rate as a function of cloud droplet number concentration ($N$). Values are averaged over the last two hours of 8-h nocturnal simulations. Cloud droplet concentration is weighted by the liquid water mass in each grid box to compute a domain average. Entrainment rate is calculated as $\Delta z_{\rm i}/\Delta t + D z_{\rm i}$, where $z_i$ is the horizontally averaged inversion height and $D$ is the large-scale divergence of the horizontal winds. The $z_i$ rate of change is calculated using the difference between the initial conditions and the average over the last 2 hours of each simulation. The curves for different meteorological conditions are labeled as described in the main text. Entrainment rates in the model simulations are consistent with the corresponding observations: at average droplet concentrations of $\sim$150 and 100 cm$^{-3}$ measured in the DYCOMS-II and ASTEX cases, the entrainment rates were estimated to be 0.38$\pm$0.04 cm s$^{-1}$ and 0.7$\pm$0.3 cm s$^{-1}$, respectively[13, 11].

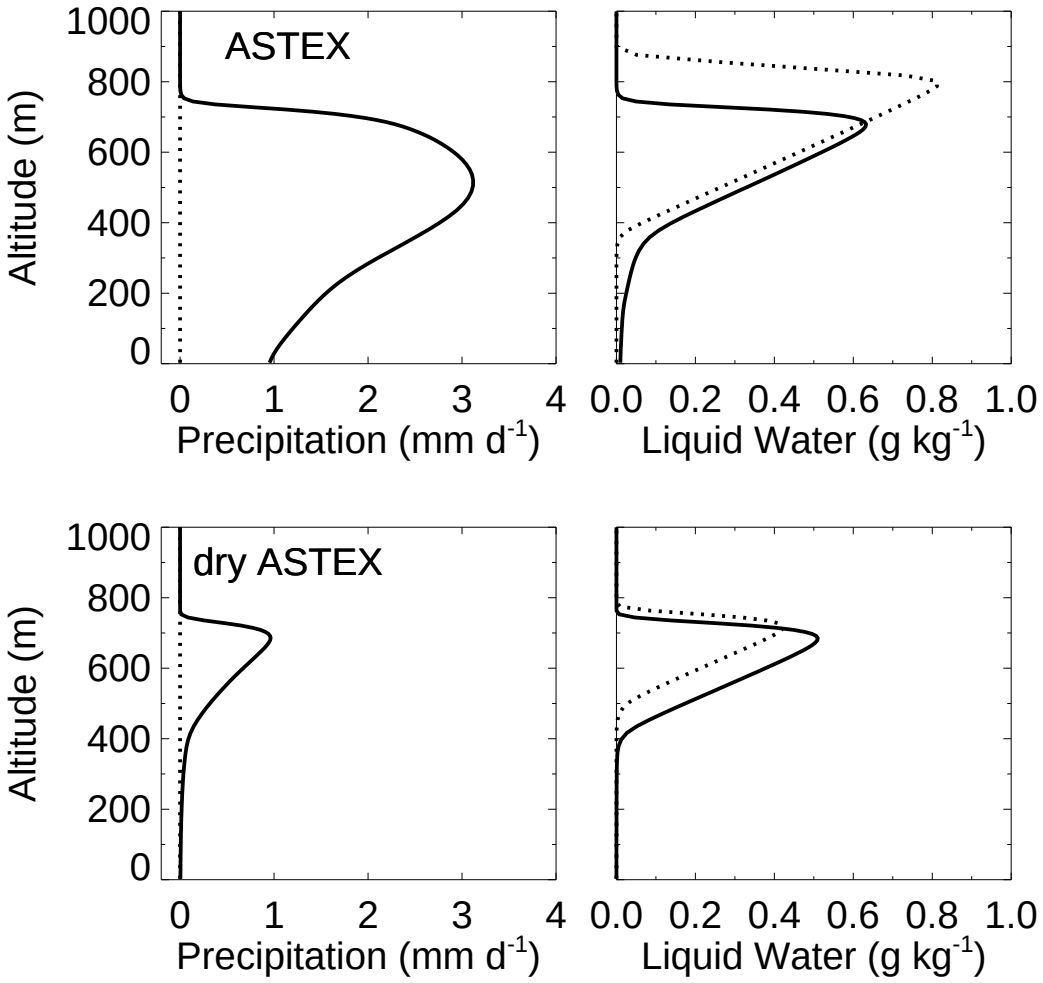


Figure 2: Horizontally averaged profiles of precipitation rate and liquid water mixing ratio averaged over the last two hours of 8-h simulations. Top panels are for the baseline (observed) ASTEX conditions, and bottom panels are for the ASTEX case with the relative humidity reduced above the boundary layer (see main text). Dotted lines are for simulations without precipitation, and solid lines are for simulations at an aerosol concentration of 150 $cm^{-3}$ (average droplet concentration of $\sim$100 $cm^{-3}$, as observed[11]) that include precipitation. For the dry ASTEX case, like the DYCOMS-II simulations at a comparable droplet concentration, the precipitation is dominated by the sedimentation of cloud droplets rather than larger drops because the collision-coalescence process is inhibited under these conditions; a similar precipitation profile was measured (with an average droplet concentration of $\sim$150 $cm^{-3}$) during the conditions on which our DYCOMS-II simulations are based[13].